NMR Evidence for Multiple Conformations in a Highly Helical Model Peptide†

Gene Merutka,‡ Dimitrios Morikis, Rafael Brüschweiler, and Peter E. Wright*

Department of Molecular Biology, The Scripps Research Institute, 10666 North Torrey Pines Road, La Jolla, California 92037

Received July 19, 1993; Revised Manuscript Received September 27, 1993®

ABSTRACT: A monomeric model peptide, acetyl-WEAQAREALAKEAAARA-amide, has been structurally characterized using the complementary techniques of ^{1}H 2D NMR and circular dichroism. Temperature-dependent CD measurements are consistent with a two-state helix/coil transition model and indicate a 65% contribution of helical conformers at 5 °C. Homonuclear 2D NMR experiments allowed the assignment of all proton resonances. The analysis of NOE-type cross-relaxation data established a large number of specific short- and medium-range NOE connectivities throughout the peptide, confirming the highly helical character of the peptide. However, the observation of long-range NOEs between the methyl protons of leucine-9 and backbone and side-chain protons of amino acids located at the N-terminus, as well as other unusual NOEs, unambiguously reflects the existence of significantly populated nonhelical structured conformers, indicating a multiconformational equilibrium. Implications of these observations with regard to secondary structure quantitation and current method limitations are discussed.

Over the last few years, much effort has been directed toward elucidating factors important in the protein folding process. One approach focuses on investigating protein fragments which might adopt nativelike structures. Initially, little structure was found in such fragments (Epand & Scheraga, 1968) until Brown and Klee (1971) discovered residual helical structure in a peptide corresponding to the N-terminal helix of the protein ribonuclease A. More recently, additional examples have been found of peptide protein fragments exhibiting secondary structure (Dyson et al., 1985, 1988a,b, 1992; Peña et al., 1989; Goodman & Kim, 1989; Waltho et al., 1989, 1993; Bruch et al., 1991). Better understanding of the factors important in stabilizing these isolated pieces of secondary structure, particularly helices, has been the focus of several recent studies. Important contributions originate from charge–helix macrodipole interactions, side-chain ion-pair electrostatics, and the inherent propensity of an amino acid to stabilize a helix [see Scholtz and Baldwin (1992) and references cited therein]. A prerequisite for the understanding of the relative weights of these contributions is a detailed characterization of the peptide conformations populated under various conditions.

Quantitation of peptide helical structure is often estimated using circular dichroism (CD)[1] with the resulting spectra interpreted on the basis of a two-state transition model. Circular dichroism spectra reflect the peptide ensemble average of the alignment of the dipoles of the helix backbone. Theoretically, this technique can be used to quantitatively compare the effects of peptide sequence alterations on helicity. However, the inability to observe experimentally the complete structural transition of peptides and the large differences in estimates of the ellipticity value for a "100%" helical state have made CD a semiquantitative technique at best.

NMR spectroscopy, on the other hand, is well suited to study local structure altered by sequence modification or experimental conditions (temperature, pH, ionic strength, and solvents). Heretofore, NMR has been applied to linear peptides rather qualitatively to characterize peptide secondary structure via amide and $C^\alpha H$ chemical shift analysis, amide proton temperature coefficients, hydrogen exchange, $^3J_{HN\alpha}$ coupling constants, and the presence of short- and medium-range NOE connectivities consistent with folded structure (Dyson & Wright, 1991).

The current work describes a detailed NMR and CD analysis of a variant of a model peptide previously found to be monomeric and apparently completely helical by CD (Merutka et al., 1991). Substitutions were made at three positions (Ala-4 to Gln, Ala-9 to Leu, and Arg-11 to Lys) to reduce the anticipated overlap in the NMR spectrum while still preserving the highly helical nature of the peptide. The resulting peptide, termed Q4L9, is Ac-WEAQAREALAKEAAARA-NH_2. It is the long-term goal of these studies to characterize a model secondary structure by complementary biophysical techniques (CD and NMR) in order to increase the insight into the potentials and limitations of the methods themselves, to better characterize and understand populated substates, and to obtain more quantitative estimates of secondary structure.

MATERIALS AND METHODS

Peptide Synthesis and Characterization. Peptide Q4L9 was manually synthesized on a *p*-methylbenzhydrylamine resin using the *in situ* neutralization method of Schnölzer et al. (1992). *N*-Methylpyrrolidone was used in the washing, activation, and coupling steps. For each 1 mmol of amino acid used in the coupling reaction, 0.95 mmol of 2-(1*H*-benzotriazol-1-yl)-1,1,3,3-tetramethyluronium hexafluorophosphate (HBTU), 0.95 mmol of 1-hydroxybenzotriazole (HOBT), and 1.5 mmol of diisopropylethylamine (DIEA) were used. HBTU was obtained from Richelieu Biotech-

† Supported by Grant GM38794 and Postdoctoral Award GM14526 (G.M.) from the National Institutes of Health and by a scholarship from the Swiss National Science Foundation (R.B.).

‡ Present address: Trimeris, Inc., Two University Place, Durham, NC 27707.

® Abstract published in *Advance ACS Abstracts*, November 15, 1993.

[1] Abbreviations: HPLC, high-pressure liquid chromatography; NMR, nuclear magnetic resonance; CD, circular dichroism; NOE, nuclear Overhauser effect; NOESY, two-dimensional nuclear Overhauser effect spectroscopy; TOCSY, two-dimensional total correlation spectroscopy; 2Q, two-dimensional double quantum spectroscopy; 2QF COSY, two-dimensional double quantum filtered correlated spectroscopy; ROESY, two-dimensional rotating-frame NOE spectroscopy; $d_{\alpha N}(i,j)$, $d_{NN}(i,j)$, etc., intramolecular distance between protons $C^\alpha H$ and NH, NH and NH, etc. of residues *i* and *j*; ppm, parts per million.

0006-2960/93/0432-13089$04.00/0

nologies (Quebec, Canada); HOBT, DIEA, and *p*-cresol were obtained from Aldrich; and Boc amino acids were obtained from Peptides International (Louisville, KY). All solvents used were HPLC grade or better. The peptide was acetylated at the N-terminus with acetic anhydride in dimethylformamide containing an equivalent of diisopropylethylamine and cleaved from the resin using standard procedures (HF:*p*-cresol ratio of 90:10, 0 °C for 1 h). The peptide was purified by reversed-phase HPLC using a Hamilton PRP-3 semipreparative column and an acetonitrile/water gradient containing 0.1% trifluoroacetic acid. Purified peptide eluted as a single peak on an analytical column, and the mass:charge ratio using fast-atom bombardment mass spectrometry was within one mass unit of that expected.

Circular Dichroism. Circular dichroism spectra were measured with an Aviv Associates Model 61DS spectropolarimeter containing a thermostable cell holder. All measurements were made at pH 5.0 ± 0.1 and are expressed as mean residue ellipticity, $[\theta]$, in units of degrees centimeter squared per decimole. Peptide concentration was determined by measuring the tryptophan maximum absorbance of a dilution into 6 M guanidine hydrochloride of a concentrated peptide stock solution. An extinction coefficient of 5690 M^{-1} cm^{-1} reported for *N*-acetyltryptophanamide at 280.8 nm (Edelhoch, 1967) was used. Sample concentration was typically about 20 μM, and the cell path length was 10 mm unless otherwise noted. Concentration dependency studies were done using cell path lengths ranging from 0.2 to 10 mm and peptide concentrations from 2 to 1800 μM at 5 and 60 °C. Single scans were obtained by taking points every 0.5 nm with a 4-s time constant and a bandwidth of 1.5 nm. Base-line-corrected spectra were smoothed using a third-order least-squares polynomial with a window size between 6 and 15 points. The absolute ellipticity of the instrument was calibrated using *d*-10-camphorsulfonic acid at 290.5 nm (Johnson, 1985) and the wavelength calibrated to within 0.1 nm using the 252.9-, 258.8,-, 260.0-, and 266.7-nm lines of benzene vapor.

Nuclear Magnetic Resonance. All NMR samples were prepared in 90% ^1H_2O/10% ^2H_2O. The pH was adjusted to pH 5.0 ± 0.1 by addition of concentrated HCl or NaOH. Values reported are pH meter readings uncorrected for the deuterium isotope effect.

NMR spectra were collected on Bruker 500- and 600-MHz AMX spectrometers. Low-power irradiation of the water signal was applied during the relaxation delay, as well as during the mixing time in the case of the NOESY experiments. All spectra are referenced with respect to water (4.963 ppm at 278 K). Two-dimensional NMR spectra were recorded in the phase-sensitive mode using time-proportional phase incrementation (TPPI) (Redfield & Kunz, 1975; Marion & Wüthrich, 1983). Assignments were made from NOESY (400-ms mixing time), TOCSY (60-ms mixing time), and double quantum spectra (30-ms mixing time) collected at 600 MHz. NOESY and TOCSY spectra were collected with a minimum of 512 experiments (900 and 1000 experiments, respectively, for assignments) of 32 scans each. Spectral widths were set to 12 500 and 7000 Hz in the ω_2 and ω_1 dimensions, respectively, with the time domain in ω_2 set to 8K points. The double quantum spectrum was recorded with 1000 t_1 points of 32 scans each and spectral widths of 7000 and 14 000 Hz in the ω_2 and ω_1 dimensions, respectively, and 4K points in t_2. The recycling delay in all experiments was set to either 1.6 or 1.8 s. Data were collected using sine modulation in t_1 (Marion & Bax, 1988). NOESY and TOCSY spectra were acquired using a Hahn echo to eliminate the need for phase and base-line correction along ω_2 (Rance & Byrd, 1983).

Temperature coefficients were measured at 288, 298, 308, and 318 K using fast TOCSY spectra (60-ms mixing time at 600 MHz) as described above but with four scans and without Hahn echo. Total data collection time for each fast- TOCSY experiment was about 1 h. Spectra were referenced to the frequency of water at the respective temperatures.

ROESY spectra were collected at 500 MHz at 275 K at various mixing times (50, 100, 150, and 200 ms) with 750 experiments of 32 scans each. Spectral widths were set to 12 500 and 7000 Hz in the ω_2 and ω_1 dimensions, respectively, with 8K points in the t_2 domain. The recycling delay was set to 1.6 s, and data were collected using sine modulation in ω_1.

Scalar $J_{HN\alpha}$ coupling constants were measured using both 1D and 2QF COSY spectra at 500 or 600 MHz. Cross sections of COSY cross-peaks with increased digital resolution (32K points) were analyzed along ω_2. The separations between antiphase absorptive and dispersive peak extrema were extracted and translated into *J* coupling constants using the method of Kim and Prestegard (1989). 1D in-phase doublets were resolution-enhanced by apodization with an increasing exponential followed by a skewed cosine-bell function.

Data were processed on Convex C240 or SUN 4 computers using FTNMR or FELIX (versions 1.1 and 2.0) software provided by Dr. Dennis Hare. Apodization using Lorentzian to Gaussian transformation or shifted sine-bell window functions was applied in both dimensions, and data were zero-filled to 4096 points prior to Fourier transformation in t_1. Linear base-line correction was applied to all spectra along ω_2.

Analytical Ultracentrifugation. Data were collected on a Beckman XL-A analytical ultracentrifuge running at 35 000 rpm and 20 °C. A dilute sample (0.1 mM) was run using a 12-mm path length centerpiece and measured at 276 nm, and the concentrated sample (5 mM) used a 3-mm centerpiece and was measured at 301 nm. The data were fit to a single ideal species model, as well as monomer–dimer and monomer–tetramer models using a nonlinear least-squares data analysis algorithm. A partial specific volume of 0.731 mL/g and a solvent density of 1.00 g/mL were used for calculations.

RESULTS

Aggregation Tests. Although the parent peptide (Marqusee & Baldwin, 1987; Merutka et al., 1991) was designed to be monomeric by uniformly displaying charged residues when in a helical conformation, introduction of tryptophan at position 1 and leucine at position 9 in Q4L9 raised the possibility of peptide aggregation. The molar ellipticity at 222 nm is independent of concentration from 2 to 1800 μM and at two different temperatures (5 and 60 °C). The state of association was determined independently using analytical ultracentrifugation at 20 °C. Dilute and concentrated peptide solutions (0.1 and 5 mM, respectively) displayed nonassociative behavior and gave monomer molecular masses of 2053 and 2196 g/mol, respectively. The molecular mass determined by FAB-mass spectroscopy, 1881 g/mol, is within the expected error of the centrifugation results. These experiments confirm that peptide Q4L9 does not form a stable aggregate at the concentrations used in this study.

Circular Dichroism. Circular dichroism spectra of peptide Q4L9 as a function of temperature are shown in Figure 1A. At low temperature, the spectrum exhibits characteristics of a helical structure, having a maximum at about 195 nm and double minima at 208 and 222 nm (Holzwarth & Doty, 1965). As the temperature is increased, the resulting spectra indicate

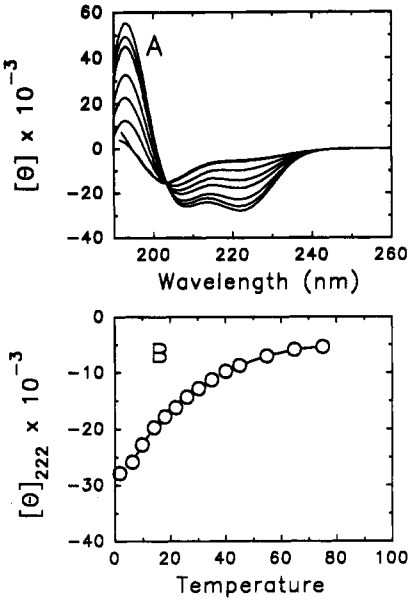

FIGURE 1: CD spectra of Q4L9 (Ac-WEAQAREALAKEAAARA-NH_2) as a function of temperature. Panel A shows the spectra at various temperatures (reading upward at 222 nm: 2, 6, 10, 18, 26, 40, and 75 °C). Panel B displays the dependence of the molar ellipticity at 222 nm with respect to temperature. The peptide concentration was 15 μM, and samples contained 1 mM phosphate buffer at pH 5.0.

a gradually more disordered conformation (Woody, 1992). The existence of an isodichroic point at 203 nm is consistent with a Zimm–Bragg-type peptide structure model.

Resonance Assignment and Spin System Identification. Complete proton resonance assignments were made using TOCSY, double quantum, and NOESY spectra following standard procedures [e.g., see Chazin et al. (1988)]. Intraresidue spin systems initially were identified using connectivities in the TOCSY spectrum, and the fingerprint region of this spectrum is well resolved with respect to the different spin systems (Figure 2). This region of the spectrum also allows identification of nitrogen side-chain protons of Arg-6, Lys-11, and Arg-16. The N^{η} protons in each arginine side chain were found, as expected, to form intraresidue exchange cross-peaks with each other in the ROESY spectrum. The N^{η} protons for both arginines were correlated to the rest of the side chain using NOESY and ROESY spectra. The NOESY spectrum was also used to link the side-chain ring

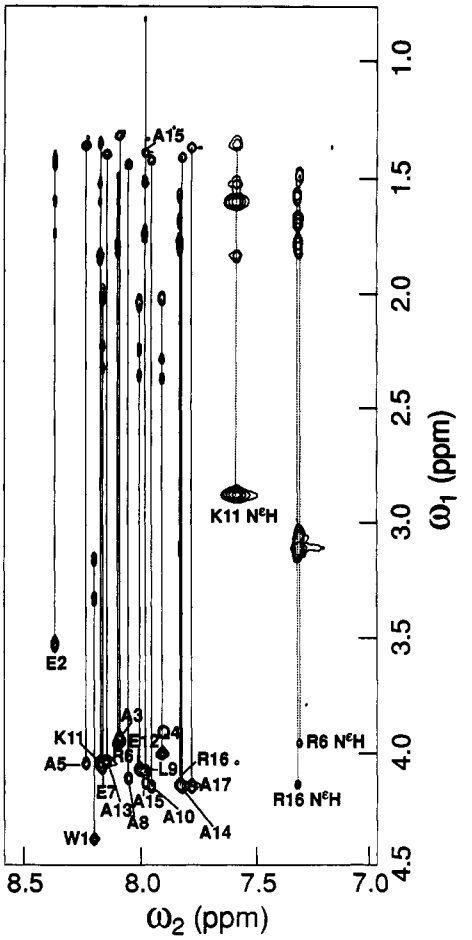

FIGURE 2: Portion of a 600-MHz TOCSY spectrum with a mixing time of 60 ms for spin system identification. Vertical lines connect the cross-peaks of spins within the same amino acid. The spectrum was measured at pH 5.0 and 278 K.

of Trp-1 to the rest of its spin system. The two N^{ϵ} protons of Gln-4 were identified in the TOCSY spectrum (data not shown).

The two nearly degenerate methyls of Leu-9 (0.845 and 0.860 ppm), which were unresolvable in TOCSY and NOESY spectra, were resolved using the double quantum spectrum. Direct connectivities at ($\omega_2 = \omega_\gamma$ or ω_δ, $\omega_1 = \omega_\gamma + \omega_\delta$) and remote connectivities at ($\omega_2 = \omega_\gamma$, $\omega_1 = \omega_\delta + \omega_\beta$) and ($\omega_2 =$

Table I: ^{1}H NMR Chemical Shifts (ppm) of Q4L9 (pH 5.0, 278 K)[a]

residue	NH	$C^{\alpha}H$	$C^{\beta}H$	$C^{\gamma}H$	$C^{\delta}H$	other
acetyl						2.030 (CH_3)
Trp-1	8.220	4.390	3.190, 3.360			10.180 ($N^{\epsilon}H$); 7.310 ($C^{\delta 1}H$); 7.415 ($C^{\epsilon 3}H$); 7.020 ($C^{\zeta 3}H$); 7.125 ($C^{\eta 2}H$); 7.410 ($C^{\zeta 2}H$)
Glu-2	8.385	3.550	1.455, 1.625	1.425, 1.770		
Ala-3	8.105	3.955	1.340			
Gln-4	7.925	4.025	2.050, 2.050	2.320, 2.400		6.870, 7.520 ($N^{\epsilon}H$)
Ala-5	8.250	4.065	1.385			
Arg-6	8.110	3.975	1.805, 1.850	1.515, 1.715	3.090, 3.145	7.335 ($N^{\epsilon}H$); 6.480, 6.905 ($N^{\eta}H$)
Glu-7	8.180	4.085	2.020, 2.045	2.265, 2.355		
Ala-8	8.070	4.130	1.465			
Leu-9	7.995	4.100	1.545, 1.780	1.735	0.845, 0.860	
Ala-10	7.970	4.165	1.450			
Lys-11	8.190	4.060	1.870, 1.870	1.375, 1.550	1.635, 1.635	2.910, 2.910 ($C^{\epsilon}H$); 7.600 ($N^{\zeta}H_3$)
Glu-12	8.020	4.090	2.070, 2.070	2.280, 2.390		
Ala-13	8.160	4.055	1.420			
Ala-14	7.995	4.150	1.415			
Ala-15	7.835	4.165	1.435			
Arg-16	7.845	4.155	1.825, 1.825	1.605, 1.715	3.130, 3.155	7.340 ($N^{\epsilon}H$); 6.490, 6.915 ($N^{\eta}H$)
Ala-17	7.795	4.160	1.390			
NH_2	7.195, 7.290					

[a] Chemical shifts are referenced to the H_2O resonance at 278 K (4.963 ppm). Chemical shifts have errors of ±0.005 ppm.

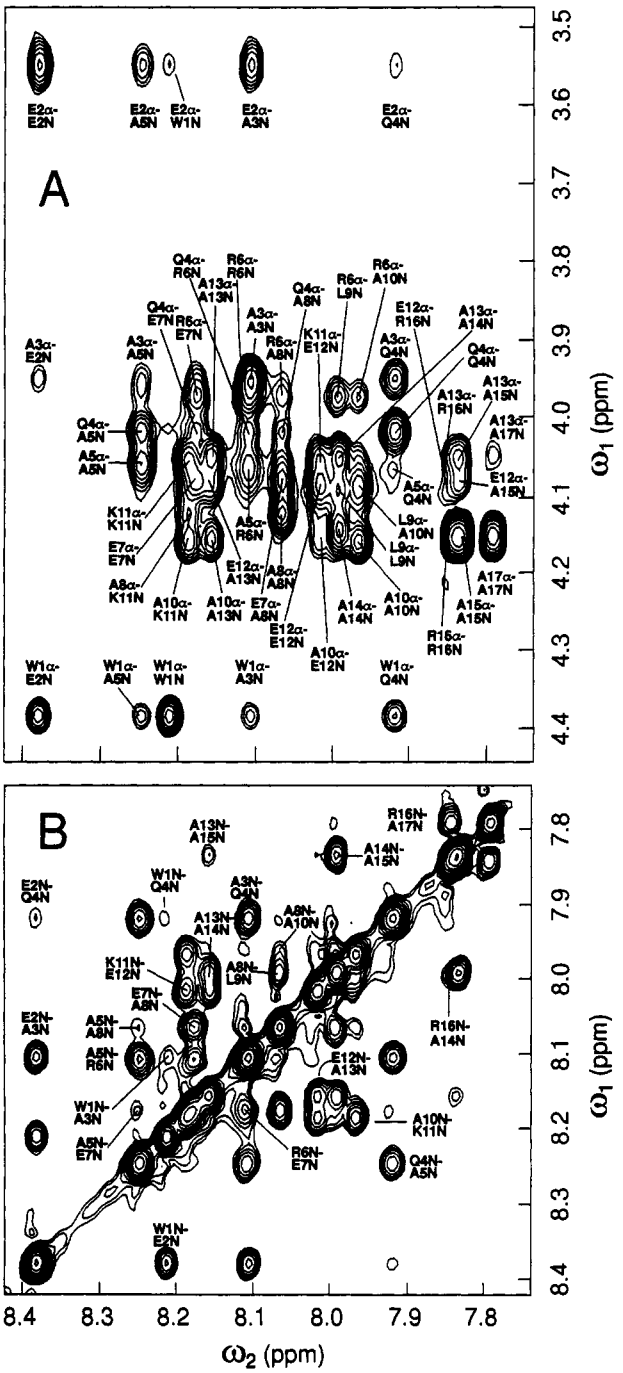

FIGURE 3: Portions of a 600-MHz NOESY spectrum with a mixing time of 400 ms at 278 K. Sequential $d_{\alpha N}$ connectivities are indicated in panel A whereas d_{NN} connectivities are displayed in panel B. The same connectivities were obtained at shorter mixing times (50, 100, and 200 ms).

$\omega_\gamma, \omega_1 = \omega_{\delta 1} + \omega_{\delta 2}$) are characteristic of two overlapping methyl resonances. However, the methyl frequencies could be distinguished using the forbidden combination cross-peaks at ($\omega_2 = \omega_{\delta 1}$, $\omega_1 = 3\omega_{\delta 1} - \omega_\gamma$) and ($\omega_2 = \omega_{\delta 2}$, $\omega_1 = 3\omega_{\delta 2} - \omega_\gamma$), which arise from differential intramethyl relaxation (Müller et al., 1987; Kay et al., 1988; Rance et al., 1989). All proton correlations were cross-checked, and methylene proton assignments were completed using the double quantum spectrum.

Sequence-Specific Assignments. Sequential assignments were made using short- and medium-range NOE connectivities initially from a 400-ms spectrum and subsequently from a 100-ms NOESY spectrum following standard procedures (Wüthrich, 1986). Complete sequence-specific assignments at 278 K, pH 5.0 in H_2O, are listed in Table I. The backbone C^αH–NH and NH–NH regions of a 400-ms NOESY

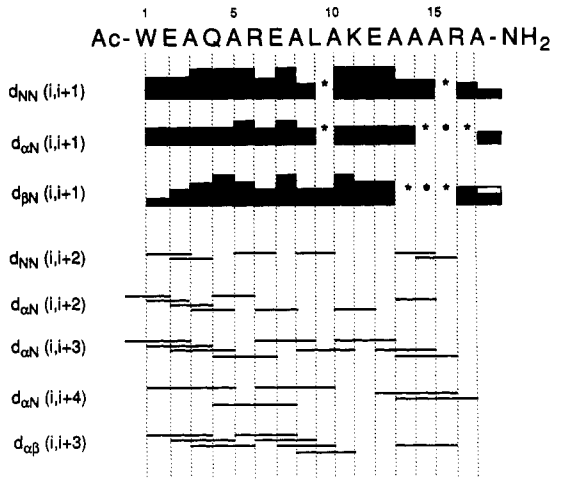

FIGURE 4: Summary of the interresidue NOEs for Q4L9 at 278 K. The varying heights of the filled bars correspond qualitatively to the relative volumes of the NOEs. The unfilled bar corresponds to the NOE volume between Ala-17 and one of the two protons in the C-terminal amide blocking group. Asterisks indicate connectivities which could not be resolved due to overlap. Data were obtained from a 600-MHz NOESY spectrum with a mixing time of 400 ms. Connectivities and relative cross-peak volumes were confirmed with a NOESY spectrum collected with a shorter mixing time of 100 ms.

spectrum are displayed in panels A and B, respectively, of Figure 3. Short- and medium-range backbone NOEs, including NH–NH(i,i+1) and -(i,i+2), C^αH–NH(i,i+1), -(i,i+3), -(i,i+4), and -(i,i+2), and C^αH–C^βH(i,i+3), are observed and are summarized in Figure 4. All asterisks and gaps in Figure 4 indicate resonance overlap which precludes unambiguous assignment. The varying bar heights of the short-range NOE connectivities correspond to relative NOE volumes. The presence of NH–NH(i,i+1) and C^βH–NH(i,i+1) NOE connectivities indicates that peptide Q4L9 contains a significant population of conformers with dihedral angles in the α-region of (ϕ,ψ) space (Billeter et al., 1982; Wüthrich et al., 1984; Dyson & Wright, 1991). Furthermore, the presence of medium-range NOE connectivities [C^αH–NH(i,i+3) and -(i,i+4), and C^αH–C^βH(i,i+3)] throughout the length of the peptide reflects a significant population of helical conformers (Wüthrich et al., 1984; Wüthrich, 1986).

Unusual Long-Range NOEs. Additional long-range NOEs were observed between the methyls of Leu-9 and the ring protons of Trp-1 as well as the backbone amide protons of residues 5–11, as shown in Figure 5. NOE cross-peaks to the ring protons are strong even at mixing times as short as 50 ms (Figure 6). NOE buildup curves involving Leu-9 methyls are comparable to those for other NOE cross-peaks (Figure 6). The behavior of all NOE intensities shown makes clear that these connectivities are not caused by spin diffusion. Other unusual NOEs involving backbone amides and side-chain C^βH and C^γH protons are shown in Figure 5. Additional NOEs between the side-chain indole proton of Trp-1 and the C^βH protons of Gln-4, Ala-5, and Ala-8 and the C^γH protons of Glu-2 and Gln-4 are also observed (data not shown).

DISCUSSION

Circular Dichroism. The presence of a significant amount of helix in peptide Q4L9 is obvious from the CD spectra at low temperatures (Figure 1). However, circular dichroism can only give a global view of the helical population and cannot, for example, discriminate between cases in which one part of the peptide is 100% helical and the remaining part unstructured or in which the entire molecule is in dynamic equilibrium between a completely helical and a disordered state or a

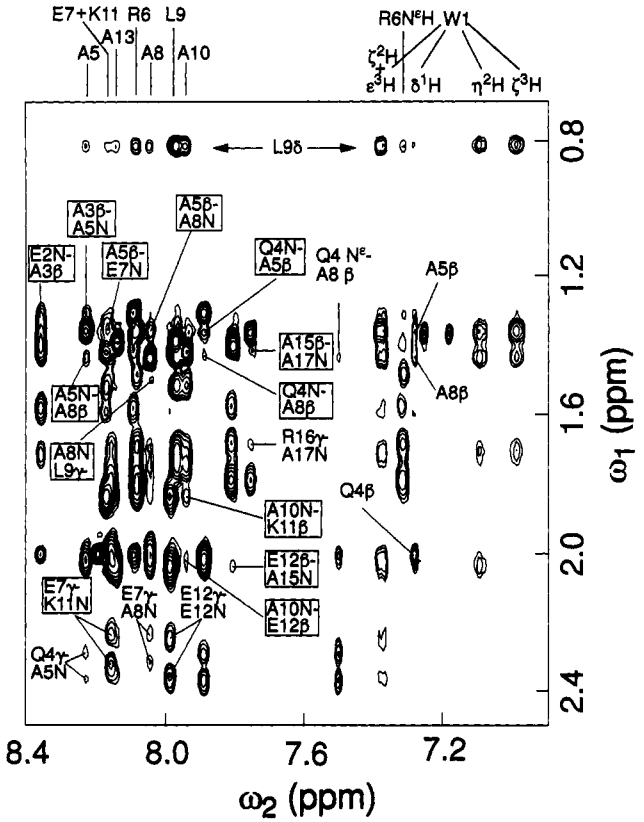

FIGURE 5: A portion of a 500-MHz spectrum with a mixing time of 200 ms taken at 275 K is displayed. Long-range interactions of the Leu-9 methyls (at about 0.83 ppm) to the Trp-1 side chain as well as backbone amide protons are indicated. The appearance of some of these cross-peaks is not consistent with an ideal α-helix. NOE connectivities not consistent with an ideal α-helix between $C^{\beta}H$ or $C^{\gamma}H$ protons and backbone amide protons are labeled within boxes.

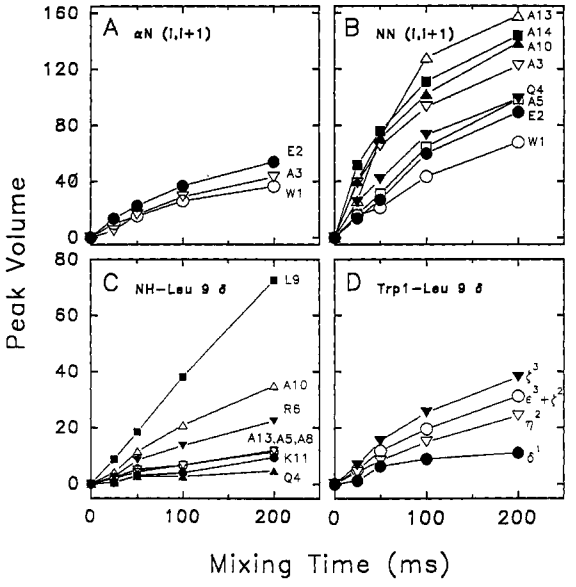

FIGURE 6: NOE buildup curves of selected cross-peaks. Panels A, B, C, and D show buildup curves of $\alpha N(i,i+1)$, $NN(i,i+1)$, backbone amide to Leu-9 $C^{\delta}H_3$, and Trp-1 side-chain protons to Leu-9 $C^{\delta}H_3$ cross-peaks, respectively. Data were obtained at 500 MHz and 275 K.

combination of both possibilities. Quantitation by circular dichroism is further complicated by the fact that there is no general consensus on the ellipticity value at 222 nm for a fully folded helix. The recent literature gives ellipticity values ranging anywhere from –28 000 to –42 000 deg cm^2 dmol^{-1}. This uncertainty originates from the difficulty of observing the complete conformational transition between the coil and the fully helical state of monomeric peptides (Merutka et al., 1990, 1991; Scholtz et al., 1991), possible contribution from aromatic side chains at 222 nm (Chakrabartty et al., 1993; Woody, 1978), and uncertainty in the length dependence of the helix signal past three turns of helix (Chen et al., 1974; Madison & Schellman, 1972; Woody & Tinoco, 1967; Manning & Woody, 1991; R. W. Woody, personal communication). Despite these uncertainties, helix propensity scales from a variety of test systems are qualitatively in agreement (Chakrabartty & Baldwin, 1992). Better quantitation might be expected by comparison with results from NMR, which provides more specific structural information at a level not obtainable by circular dichroism.

Peptide Q4L9 is estimated to be about 65% helical at 278 K using $[\theta]_{222}$ values of approximately +500 and –40 500 deg cm^2 dmol^{-1} for the disordered and completely helical states (Merutka et al., 1991; Scholtz et al., 1991). [If a value of –32 000 deg cm^2 dmol^{-1} for 100% helicity is taken (Lyu et al., 1990), the helicity estimate for Q4L9 rises to about 83%.] The helicity is significantly less than that estimated for the parent peptide Ac-W(EAAAR)$_3$A-NH$_2$, 80% helical (if 100% helicity corresponds to –40 500 deg cm^2 dmol^{-1}), under similar conditions (Merutka et al., 1991). This reduction in helical content is attributed to substitution of three residues in the parent sequence by amino acids of lower helical propensity: Ala-4 to Gln, Ala-9 to Leu, and Arg-11 to Lys [see Chakrabartty and Baldwin (1992) and references cited therein]. Fractional helix content in a peptide, as indicated by CD, is likely to originate from a mixture of completely helical, disordered, and a significant number of partially helical states. The ellipticity at 222 nm can also be influenced by distortions of the helix backbone resulting in deviation from the ideal helix hydrogen bond geometry (Manning et al., 1988). The existence of an isodichroic point (Figure 1A) suggests the system can be described with a Zimm–Bragg-type model.

NMR Chemical Shifts. Several NMR parameters provide information on the amount of secondary structure present in peptides in solution. Perhaps the most empirical method focuses on the change in chemical shift of backbone protons relative to experimental random-coil values (Bundi & Wüthrich, 1979; Wishart et al., 1991). Deviations from random-coil values of $C^{\alpha}H$ and NH protons are indicative of secondary structure (Dalgarno et al., 1983; Pardi et al., 1983; Szilágyi & Jardetzky, 1989; Williamson, 1990; Wishart et al., 1991), complementing traditional analysis using medium-range NOE connectivities (see below).

A plot of the $C^{\alpha}H$ and NH proton chemical shifts of peptide Q4L9 relative to random-coil values [at 35 °C; Bundi & Wüthrich (1979)] is shown in Figure 7. The $C^{\alpha}H$ and NH proton chemical shifts of peptide Q4L9 are shifted upfield relative to random-coil values, indicating helical structure (Szilágyi & Jardetzky, 1989; Williamson, 1990; Wishart et al., 1991). In contrast to recent reports for other helical peptides (Kuntz et al., 1991; Jiménez et al., 1992; Zhou et al., 1992), the amide proton chemical shifts of Q4L9 show no periodicity. Periodicity in chemical shift has been attributed to periodicity of hydrophobic residues (Blanco et al., 1992) and/or hydrogen bond length (Zhou et al., 1992), suggesting a curved helical structure. The lack of substantial amide chemical shift periodicity in peptide Q4L9 is probably because the peptide is not amphipathic, in contrast to most helical peptides isolated from proteins (Jiménez et al., 1992), and is consistent with a regular helical structure (Blanco et al., 1992). The chemical shift differences observed for the $C^{\alpha}H$ and NH protons at the N- and C-termini of Q4L9 are, however,

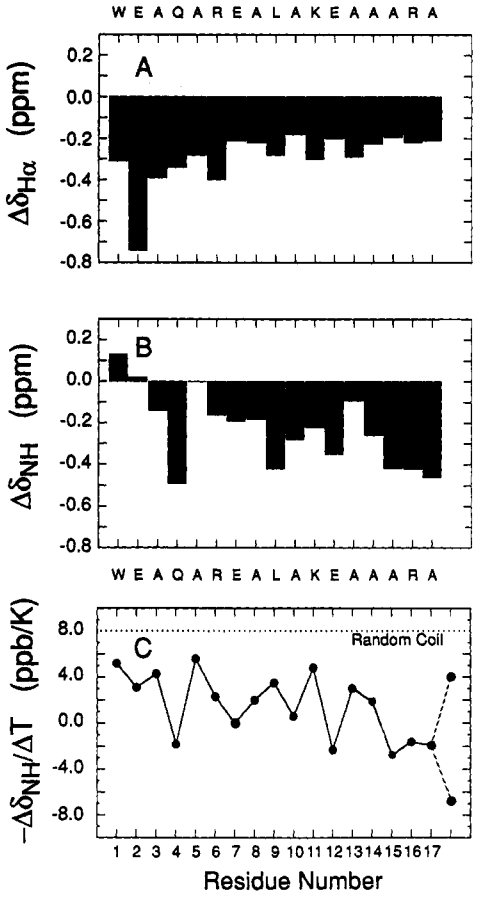

FIGURE 7: Plot of the chemical shift differences of the C$^{\alpha}$H and backbone NH protons of each residue and their random-coil value (Bundi & Wüthrich, 1979). Data were obtained at pH 5.0 and 278 K at 600 MHz. Panel C displays the measured temperature coefficients obtained from fast TOCSY spectra (60-ms mixing time) every 10 K in the temperature range 278–318 K. The dashed line in panel C corresponds to the temperature coefficient of an alanine amide in a random peptide.

consistent with the differential effect observed in helices in some proteins (Williamson, 1990); i.e., the NH protons at the C-terminus have a more upfield chemical shift than those at the N-terminus (Figure 7B); the opposite case applies to C$^{\alpha}$H protons (Figure 7A). Estimation of helicity based on C$^{\alpha}$H upfield shifts as suggested recently (Rizo et al., 1993) yields results that are comparable with the helicity values obtained by CD. Furthermore, the magnitude of the upfield shifts of the backbone NH and C$^{\alpha}$H protons is similar to theoretical C$^{\alpha}$H and NH proton chemical shifts of –0.2 to –0.3 ppm for a regular polyalanine α-helix (Blanco et al., 1992; K. Ösapay and D. A. Case, personal communication).

Quantitative structural interpretation of chemical shift data is principally restricted by the fact that different contributions, such as electrostatic effects, ring current shifts, and other magnetic anisotropies (Harris, 1986), can affect the chemical shift values significantly. Furthermore, the decomposition of the chemical shift into an intrinsic or "random coil" part and a "structural" part is justifiable from a theoretical point of view, but is difficult to realize in practice, since the "random coil" values have to be determined for the specific conditions (temperature, pH, solvent) under which the system is studied. A complete set of amino acid random-coil values in water measured at 35 °C and pH 7 has been published (Bundi & Wüthrich, 1979). Nevertheless, since amide protons are particularly sensitive to changes in environment such as temperature or pH, a more quantitative chemical shift analysis would need to take changes in random-coil values better into account. Random-coil temperature coefficients have been previously estimated for only a few residues (Jiménez et al., 1986) and can be rather large, e.g., –6.9 to –8.6 ppb/K at pH 3.0 for an alanine residue. Since random-coil chemical shifts and temperature coefficients are not available for all residues in Q4L9 at the conditions being studied, no attempt has been made to quantitate secondary structure using chemical shift data.

There are, however, irregularities in the chemical shifts of Q4L9 that suggest deviation from an ideal helical structure. The amide proton chemical shift of Ala-13 is small relative to the shifts of adjacent residues. This might reflect a distortion of the helix affecting the hydrogen bond with Leu-9 (see below for a more detailed discussion). No definitive statements can be made regarding the irregular chemical shifts of the amide protons of the first five residues (Figure 7B), since these could arise either from altered hydrogen bonding or from ring current contributions from the side chain of Trp-1. Ring currents might also explain the rather large upfield shift of the C$^{\alpha}$H carbon of Glu-2 (Figure 7A).

In summary, the upfield shifts observed for the C$^{\alpha}$H and NH resonances of Q4L9 are in general agreement with the circular dichroism results in suggesting the presence of a significant amount of helix. The chemical shift data suggest that there may be some distortions in the backbone of the N-terminus as well as around Leu-9.

Information on hydrogen-bonding interactions in peptides can be obtained by measurement of the temperature dependence of amide proton chemical shifts (Ohnishi & Urry, 1969; Dyson et al., 1988; Gellman et al., 1991). Temperature coefficients for Q4L9 are shown in Figure 7C and vary from +2.8 to –5.6 ppb/K, suggesting that some strong hydrogen bonds are formed. For comparison, the temperature coefficient of an alanine residue in a random peptide under identical conditions is –8.6 ppb/K (Merutka and Wright, in preparation).

Scalar J Couplings. A second way to estimate secondary structure relies on the use of scalar $^3J_{HN\alpha}$ coupling constants (Karplus, 1959; Bystrov, 1976). Due to strong overlap of most of the NH resonances in the 1D spectrum, an attempt was made to extract the *J* coupling constants from NH–C$^{\alpha}$H cross-peaks in the 2QF COSY spectrum according to the method of Kim and Prestegard (1989). Coupling constants were measured from spectra recorded at different temperatures to resolve resonance overlaps. The best dispersion was obtained at 298 K where 11 couplings could be resolved in the 2QF COSY spectrum, 4 of which could also be observed in 1D spectra (Figure 8). The data for Glu-2, Glu-7, Leu-9, and Ala-17 illustrate a systematic discrepancy between *J* coupling constant estimates obtained from antiphase 2D data and resolution-enhanced in-phase 1D data. In all cases, the 1D in-phase splitting is smaller than the coupling extracted from 2QF COSY cross-peaks. Only a small change in *J* coupling constants obtained from 2QF COSY spectra was observed with increasing temperature (Figure 8). This is in agreement with the slight increase of about 1 Hz of the *J* coupling constants of two always well-resolved amide protons in the 1D spectrum, Glu-2 and Glu-7, as the temperature is increased from 298 to 328 K. 1D coupling constants were not obtainable at lower temperatures due to a combination of small couplings, increased line broadening, and cross-peak overlap. Overall, the scalar $^3J_{HN\alpha}$ coupling data are consistent with other NMR data suggesting that peptide Q4L9 contains a high helical population to both the N- and C-termini.

NMR Cross-Relaxation. The most unambiguous indication of secondary structure is obtained from characteristic patterns

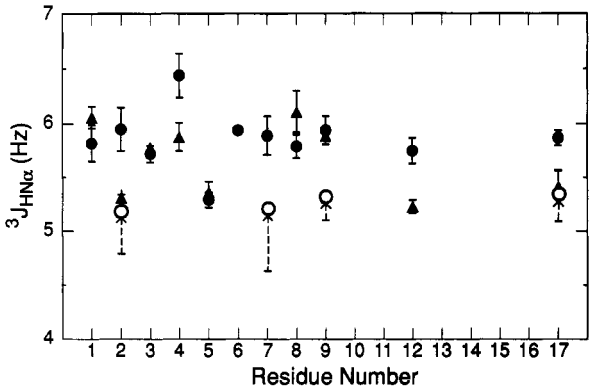

FIGURE 8: Resolvable scalar $^3J_{HN\alpha}$ coupling constants extracted from a 2QF COSY (●) at 298 K and 500 MHz, from a 1D spectrum (○) at 298 K and 600 MHz, and from a 2QF COSY spectrum (▲) at 278 K and 600 MHz are displayed. The error bars indicate the variation of J couplings extracted from the upper and lower half of the same COSY cross-peak. Coupling constants from repeat 2QF COSY experiments were found to differ by less than 0.5 Hz. J coupling constants from 1D spectra were measured after apodization with an increasing exponential followed by a skewed cosine-bell function. The dashed arrows indicate the change of the apparent splittings before and after apodization (0.3–0.6 Hz). Coupling constants from 1D spectra were not obtainable at 278 K.

of short- and medium-range NOESY cross-peaks. The observation of the intense sequential NOE connectivities NH–NH(i,i+1) and C$^\beta$H–NH(i,i+1) suggests that the peptide contains a significant population of conformers with dihedral angles in the α-region of (ϕ,ψ) space (Billeter et al., 1982; Wüthrich et al., 1984; Dyson & Wright, 1991). However, observation of additional medium-range connectivities is necessary to confirm that folded conformations are present. In the case of Q4L9, medium-range NOE connectivities [C$^\alpha$H–NH(i,i+3), C$^\alpha$H–NH(i,i+4), and C$^\alpha$H–C$^\beta$H(i,i+3)] along the entire peptide backbone provide unambiguous evidence for a significant population of helical conformers. These medium-range NOEs extend to both the N- and C-termini, suggesting that the helix is not extensively frayed at the termini. This is in contrast to what has been assumed for highly helical peptides of similar sequence (Chakrabartty et al., 1993) and is in contrast to most other peptide helical systems in which medium-range connectivities to the termini are not observed either in aqueous systems (Dyson et al., 1988, 1992; Waltho et al., 1989, 1993; Bradley et al., 1990) or in the helix-stabilizing solvent trifluoroethanol (Dyson et al., 1988; Storrs et al., 1992). However a small extent of end-fraying is suggested by the relative intensity of the resolvable C$^\alpha$H–NH(i,i+3) cross-peaks; the intensities of these cross-peaks at the N-terminus (Trp-1 and Glu-2) are 60–80% of those involving residues in the middle of the helix. It is unclear whether these differences can be attributed strictly to end-fraying or whether sequence-specific interactions play a part. In contrast, intensities of C$^\alpha$H–NH(i,i+4) cross-peaks appear to be more uniform throughout the sequence.

Quantitation of the amount of helix present in peptides using cross-peak intensity ratios for NH–NH(i,i+1) and C$^\alpha$H–NH(i,i+1) NOE connectivities has been suggested by Bradley et al. (1990). This analysis is based on the simplified assumption that each amino acid is in a dynamic equilibrium between only two states, an α-helical and an extended state [β-region of (ϕ,ψ) space]. Applying this method to the NOESY data of Q4L9 reveals a calculated helix population ranging between 88 and 96% for the N-terminal half of the peptide [Trp-1, 91%; Glu-2, 90%; Ala-3, 96%; Gln-4, 94%; Ala-5, 91%; Arg-6, 88%; Glu-7, 88%; Ala-10, 94%; Lys-11, 93%; Glu-12, 92%; Ala-17, 72% and 81% (for the two protons of the terminal NH_2 blocking group)]. Data are not available for all residues due to spectral overlap. The above analysis includes integration of four spectra measured at different field strengths and different NOESY mixing times (100-ms mixing time at 500 MHz and 100-, 200-, and 400-ms mixing times at 600 MHz, respectively). The experimental error in these helicity estimates ranges between 1% and 4%. This analysis confirms the conclusion from the NOE connectivity diagram (Figure 4) that backbone dihedral angles in the α-helical region of (ϕ,ψ) space extend to both termini. However, the very high average helicity calculated is inconsistent with both the $^3J_{HN\alpha}$ coupling constant and the CD data. Considering that the underlying two-state model is not very realistic, the calculated helicity using these simple NOE ratios in the above method should not be taken too literally.

The above discussion involving chemical shift changes, $^3J_{HN\alpha}$ coupling constants, NOE volume ratios, and medium-range connectivities gives little indication that other nonhelical structured states are present. However, the CD data suggest that Q4L9 is not fully helical. A more detailed examination of the NMR data also provides evidence for distortions from a regular α-helical structure, since long-range NOE connectivities are observed between the Leu-9 methyls and the side chain of Trp-1 (Figure 5). Molecular modeling shows that extreme back-folding of the Trp-1 side chain onto the helix backbone accompanied by suitable orientation of the Leu-9 side chain can bring the Trp-1 C$^{\eta 2}$H and C$^{\zeta 3}$H protons into a 4-Å range of the Leu-9 C$^\delta$H$_3$ protons. At the same time, however, the distance to Trp-1 N$^\epsilon$H and C$^\delta$H is in the range of 6–9 Å. Similarly, the side chain of Leu-9 cannot satisfy simultaneously NOEs to the Trp-1 side chain, the Leu-2 C$^\alpha$H proton (data not shown), and the NH proton of Ala-13. Thus, the NOE spectrum is incompatible with the static helix model.

Potential interpretations of these NOEs are extended spin diffusion along the helix axis, aggregation, anisotropic tumbling, or the presence of additional and more flexible backbone conformations. Spin diffusion can be excluded since these long-range NOEs are present at even very short mixing times and are also part of the linear portion of the NOE buildup curve (Figure 6C,D). The concentration independence of the CD signal and analytical ultracentrifugation results indicate that Q4L9 is monomeric at NMR concentrations. If the Trp-1 to Leu-9 NOEs were due to anisotropic tumbling, additional long-range NOEs between other pairs of side-chain protons along the helix axis would be expected, but are not observed. The most likely explanation is therefore the occurrence of multiple conformations involving a helical backbone structure and at least one alternative backbone conformation, allowing the clustering of Leu-9 with the N-terminal side chains. Weak and medium strength backbone NOEs are also observed that are not entirely consistent with a regular α-helix: NH–C$^\alpha$H-(i,i+1) for Trp-1 and Glu-2 and NH–NH(i,i+3) for Trp-1 (Figure 3) as well as numerous interactions involving the NH or C$^\beta$H protons of residues Ala-5 and Ala-8 (Figure 5). The proton–proton distances for these unusual NOEs range between 4.5 and 8 Å in a regular α-helix (Wüthrich et al., 1984). These interactions clearly depict the presence of one or more nonhelical substates, perhaps involving a bend in the N-terminus, which would be missed in a traditional analysis solely based on backbone connectivities. Other unusual NOEs involving amide backbone and C$^\beta$H protons are also observed to a lesser extent in the C-terminal region of the peptide, suggesting backbone distortions in this region as well.

It has been suggested that short alanine peptides of similar sequence may be predominantly 3_{10}-helical instead of α-helical (Miick et al., 1992). However, our CD and NMR results on Q4L9 do not support this conclusion. Calculated CD spectra

for the α-helix and 3_{10}-helix suggest that although both types of helices have similar intensities at 222 nm, a 3_{10}-helix should have a much more intense band at 208 nm than at 222 nm (Manning & Woody, 1991). Thus, CD data imply that Q4L9 is predominantly α-helix rather than 3_{10}-helix, as indicated in Figure 1A.

A cursory NMR analysis cannot readily distinguish the relative populations of α- and 3_{10}-helical structures. Static model calculations show that α- and 3_{10}-helices give rise to rather similar NMR observables (Wüthrich et al., 1984; Wagner et al., 1986). Therefore, distinction and quantitation of these two types of helix using experimental NMR data would need to take into account also motional effects such as local flexibility and multiple conformations. Qualitatively, the presence of $C^{\alpha}H$–$C^{\beta}H(i,i+3)$ and $C^{\alpha}H$–$NH(i,i+3)$ NOE connectivities only indicates the presence of helix (α or 3_{10}); however, the presence of $C^{\alpha}H$–$NH(i,i+4)$ connectivities throughout the peptide (Figures 3A and 4) strongly suggests the existence of α-helical structure in peptide Q4L9. Nevertheless, since $C^{\alpha}H$–$NH(i,i+2)$ NOEs are also observed, it is possible that significant transient subpopulations of nascent or 3_{10}-helical conformations are present in the conformational ensemble, as seen in molecular dynamics simulations of helical peptides in aqueous solution (Daggett & Levitt, 1992; Soman et al., 1991; Tirado-Rives & Jorgensen, 1991).

CONCLUSIONS

Although both biophysical methods, CD and NMR, used in the present work are well suited for a qualitative estimation of secondary structure, a quantitative analysis is significantly more complex. Translation of observed NOE intensities into an ensemble of interconverting structures is by no means trivial. Procedures used for the generation of protein structures on the basis of NMR data based on distance geometry (Havel & Wüthrich, 1984; Braun & Go, 1985) or restrained molecular dynamics (Kaptein et al., 1985; Clore et al., 1985) tend to fail to describe a multiconformational equilibrium since they bias the conformational search toward a single static structure that simultaneously satisfies as best as possible all of the ensemble-averaged experimental data. More recently, protocols have been developed and applied (Torda et al., 1990; Brüschweiler et al., 1991) using an NMR constraint-driven search of conformational space to explain experimental data in terms of true ensemble averages. Extension of such protocols to helical peptides is likely to improve the quantitative characterization of conformational ensembles of linear peptides.

CD, on the other hand, probes the peptide conformational ensemble in a rather low-dimensional conformational subspace that emphasizes the occurrence of aligned electric dipoles. CD might indicate but cannot further characterize structural substates. The appearance of an isodichroic point for peptide Q4L9, in Figure 1A, for example, is consistent with but does not prove a two-state helix/coil transition. CD, however, does not allow further structural characterization of nonhelical substates involving interactions between Trp-1 and Leu-9.

In the present study, we have shown that a "standard"-type analysis of the NMR data suggests a highly helical molecule but gives little information on helix quantitation and does not allow conclusions regarding the presence of nonhelical or distorted helical, well-structured peptide substates. CD data suggest a high degree of overall helicity but at the same time unambiguously indicate that the molecule is not completely helical. This observation is supported by detailed examination of the NMR spectrum, in particular the region involving side-chain NOEs, revealing the presence of non-α-helical conformers. It is uncertain at this point whether the presence of Trp-1 and Leu-9 causes the formation of nonhelical or distorted helical substates or if these two amino acids represent fortuitous markers monitoring these nonhelical states.

It is clear that on a qualitative level CD and NMR complement each other in secondary structure characterization. Quantitatively, however, it is difficult to improve interpretation of peptide CD data beyond assuming a two-state model. This can be attributed to the uncertainties in obtaining spectroscopic reference values for well-defined conformational states. In addition, theoretical CD calculations often have difficulty in recreating both the shape and magnitude of spectra commonly attributed to a particular secondary structure (e.g., the 208- and 222-nm minima in helices) if precise dihedral angle information is not available (Manning et al., 1988; Manning & Woody, 1991). Although more work-intensive, NMR studies, on the other hand, have the potential to provide a more realistic picture of linear peptide conformational substates populated in solution. Progress in this direction requires, as suggested in this work, inclusion of all available NMR information, in particular long-range NOEs involving side-chain protons and improved computational methods that allow efficient searching of available conformational space.

ACKNOWLEDGMENT

We thank Dr. Paul Voelker and Beckman Instruments for providing analytical ultracentrifuge results.

REFERENCES

Billeter, M., Braun, W., & Wüthrich, K. (1982) *J. Mol. Biol. 155*, 321–346.
Blanco, F. J., Herranz, J., González, C., Jiménez, M. A., Rico, M., Santoro, J., & Nieto, J. L. (1992) *J. Am. Chem. Soc. 114*, 9676–9677.
Bradley, E. K., Thomasen, J. F., Cohen, F. E., Kosen, P. A., & Kuntz, I. D. (1990) *J. Mol. Biol. 215*, 607–622.
Braun, W., & Go, N. (1985) *J. Mol. Biol. 186*, 611–626.
Brown, J. E., & Klee, W. A. (1971) *Biochemistry 10*, 470–476.
Bruch, M. D., Dhingra, M. M., & Gierasch, L. M. (1991) *Proteins: Struct., Funct., Genet. 10*, 130–139.
Brüschweiler, R., Blackledge, M., & Ernst, R. R. (1991) *J. Biomol. NMR 1*, 3–11.
Bundi, A., & Wüthrich, K. (1979) *Biopolymers 18*, 285–298.
Bystrov, V. F. (1976) *Prog. NMR Spectrosc. 10*, 41–82.
Chakrabartty, A., & Baldwin, R. L. (1992) in *Protein Folding: In Vivo and In Vitro* (Cleland, J., Ed.) ACS Books, New York.
Chakrabartty, A., Kortemme, T., Padmanabhan, S., & Baldwin, R. L. (1993) *Biochemistry 32*, 5560–5565.
Chazin, W. J., Rance, M., & Wright, P. E. (1988) *J. Mol. Biol. 202*, 603–622.
Chen, Y.-H., Yang, J. T., & Chau, K. H. (1974) *Biochemistry 13*, 3350–3359.
Clore, G. M., Gronenborn, A. M., Brünger, A. T., & Karplus, M. (1985) *J. Mol. Biol. 186*, 435–455.
Daggett, V., & Levitt, M. (1992) *J. Mol. Biol. 223*, 1121–1138.
Dalgarno, D. C., Levine, B. A., & Williams, R. J. P. (1983) *Biosci. Rep. 3*, 443–452.
Dyson, H. J., & Wright, P. E. (1991) *Annu. Rev. Biophys. Chem. 20*, 519–538.
Dyson, H. J., Cross, K. J., Houghten, R. A., Wilson, I. A., Wright, P. E., & Lerner, R. A. (1985) *Nature (London) 318*, 480–483.
Dyson, H. J., Rance, M., Houghten, R. A., Lerner, R. A., & Wright, P. E. (1988a) *J. Mol. Biol. 201*, 161–200.
Dyson, H. J., Rance, M., Houghten, R. A., Wright, P. E., & Lerner, R. A. (1988b) *J. Mol. Biol. 201*, 201–218.
Dyson, H. J., Merutka, G., Waltho, J. P., Lerner, R. A., & Wright, P. E. (1992) *J. Mol. Biol. 226*, 795–817.
Edelhoch, H. (1967) *Biochemistry 6*, 1948–1954.

Epand, R. M., & Scheraga, H. A. (1968) *Biochemistry 7*, 2864–2872.
Gellman, S. H., Dado, G. P., Liang, G.-B., & Adams, B. R. (1991) *J. Am. Chem. Soc. 113*, 1164–1173.
Goodman, E. M., & Kim, P. S. (1989) *Biochemistry 28*, 4343–4347.
Harris, R. K. (1986) *Nuclear Magnetic Resonance Spectroscopy, A Physicochemical View*, Longman, Scientific & Technical, Essex, England.
Havel, T. F., & Wüthrich, K. (1984) *Bull. Math. Biol. 46*, 673–698.
Holzwarth, G., & Doty, P. (1965) *J. Am. Chem. Soc. 87*, 218–228.
Jiménez, M. A., Nieto, J. L., Rico, M., Santoro, J., Herranz, J., & Bermejo, F. J. (1986) *J. Mol. Struct. 143*, 435–438.
Jiménez, M. A., Blanco, F. J., Rico, M., Santoro, J., Herranz, J., & Nieto, J. L. (1992) *Eur. J. Biochem. 207*, 39–49.
Johnson, W. C., Jr. (1985) *Methods Biochem. Anal. 31*, 61–163.
Kaptein, R., Zuiderweg, E. R. P., Scheek, R. M., Boelens, R., & van Gunsteren, W. F. (1985) *J. Mol. Biol. 182*, 179–182.
Karplus, M. (1959) *J. Chem. Phys. 30*, 11–15.
Kay, L. E., Holak, T. A., & Prestegard, J. H. (1988) *J. Magn. Reson. 76*, 30–40.
Kim, Y., & Prestegard, J. H. (1989) *J. Magn. Reson. 84*, 9–13.
Kuntz, I. D., Kosen, P. A., & Craig, E. C. (1991) *J. Am. Chem. Soc. 113*, 1406–1408.
Lyu, P. C., Liff, M. I., Marky, L. A., & Kallenbach, N. R. (1990) *Science 250*, 669–673.
Madison, V., & Schellman, J. (1972) *Biopolymers 11*, 1041–1076.
Manning, M. C., & Woody, R. W. (1991) *Biopolymers 31*, 569–586.
Manning, M. C., Illangasekare, M., & Woody, R. W. (1988) *Biophys. Chem. 31*, 72–86.
Marion, D., & Wüthrich, K. (1983) *Biochem. Biophys. Res. Commun. 113*, 967–974.
Marion, D., & Bax, A. (1988) *J. Magn. Reson. 79*, 352–356.
Marqusee, S., & Baldwin, R. L. (1987) *Proc. Natl. Acad. Sci. U.S.A. 84*, 8898–8902.
Merutka, G., Lipton, W., Shalongo, W., Park, S.-H., & Stellwagen, E. (1990) *Biochemistry 29*, 7511–7515.
Merutka, G., Shalongo, W., & Stellwagen, E. (1991) *Biochemistry 30*, 4245–4248.
Miick, S. M., Martinez, G. V., Fiori, W. R., Todd, A. P., & Millhauser, G. L. (1992) *Nature 359*, 653–655.
Müller, N., Bodenhausen, G., & Ernst, R. R. (1987) *J. Magn. Reson. 75*, 297–334.
Ohnishi, M., & Urry, D. W. (1969) *Biochem. Biophys. Res. Commun. 36*, 194–202.
Pardi, A., Wagner, G., & Wüthrich, K. (1983) *Eur. J. Biochem. 137*, 445–454.
Peña, M. C., Rico, M., Jiménez, M. A., Herranz, J., Santoro, J., & Nieto, J. L. (1989) *Biochim. Biophys. Acta 957*, 380–389.
Rance, M., & Byrd, M. A. (1983) *J. Magn. Reson. 52*, 221–240.
Rance, M., Chazin, W., Dalvit, C., & Wright, P. E. (1989) *Methods Enzymol. 176*, 114–134.
Redfield, A. G., & Kunz, S. D. (1975) *J. Magn. Reson. 19*, 250–254.
Rizo, J., Blanco, F. J., Kobe, B., Bruch, M. D., & Gierasch, L. M. (1993) *Biochemistry 32*, 4881–4894.
Schnölzer, M., Alewood, P., Jones, A., Alewood, D., & Kent, S. B. H. (1992) *Int. J. Pept. Protein Res. 40*, 180–193.
Scholtz, J. M., & Baldwin, R. L. (1992) *Annu. Rev. Biophys. Biomol. Struct. 21*, 95–118.
Scholtz, J. M., Qian, J., York, E. J., Steward, J. M., & Baldwin, R. L. (1991) *Biopolymers 31*, 1463–1470.
Soman, K. V., Karimi, A., & Case, D. A. (1991) *Biopolymers 31*, 1351–1361.
Storrs, R. W., Truckses, D., & Wemmer, D. E. (1992) *Biopolymers 32*, 1695–1702.
Szilágyi, L., & Jardetzky, O. (1989) *J. Magn. Reson. 83*, 441–449.
Tirado-Rives, J., & Jorgensen, W. L. (1991) *Biochemistry 30*, 3864–3871.
Torda, A. E., Scheek, R. M., & van Gunsteren, W. F. (1990) *J. Mol. Biol. 214*, 223–235.
Wagner, G., Neuhaus, D., Wörgötter, E., Vasák, M., Kägi, J. H. R., & Wüthrich, K. (1986) *J. Mol. Biol. 187*, 131–135.
Waltho, J. P., Feher, V. A., Lerner, R. A., & Wright, P. E. (1989) *FEBS Lett. 250*, 400–404.
Waltho, J. P., Feher, V. A., Merutka, G., Dyson, H. J., & Wright, P. E. (1993) *Biochemistry 32*, 6337–6347.
Williamson, M. P. (1990) *Biopolymers 29*, 1423–1431.
Wishart, D. S., Sykes, B. D., & Richards, F. M. (1991) *J. Mol. Biol. 222*, 311–333.
Woody, R. W. (1978) *Biopolymers 17*, 1451–1467.
Woody, R. W. (1992) *Adv. Biophys. Chem. 2*, 37–79.
Woody, R. W., & Tinoco, I. (1967) *J. Chem. Phys. 46*, 4927–4945.
Wüthrich, K. (1986) *NMR of Proteins and Nucleic Acids*, J. Wiley, New York.
Wüthrich, K., Billeter, M., & Braun, W. (1984) *J. Mol. Biol. 180*, 715–740.
Zhou, N. E., Zhu, B.-Y., Sykes, B. D., & Hodges, R. S. (1992) *J. Am. Chem. Soc. 114*, 4320–4326.